Single-Particle Dynamics in Collisionless Magnetic Reconnection

J. Egedal and A. Fasoli

Massachusetts Institute of Technology, Plasma Science and Fusion Center, Cambridge, Massachusetts 02139

(Received 22 December 2000)

The role of single-particle dynamics in driven magnetic reconnection in collisionless plasmas is investigated experimentally and analytically. The trapping of particle orbits in the magnetic cusp is observed to allow fast reconnection in the absence of a macroscopic current layer, at a rate identical to that of vacuum. The development of an electrostatic potential structure around the magnetic X line during reconnection is predicted theoretically and observed experimentally.

DOI: 10.1103/PhysRevLett.86.5047 PACS numbers: 52.20.–j, 52.25.–b, 52.30.–q

Changes in the magnetic field topology in the presence of plasma go under the general name of magnetic reconnection [1]. Because of the coupling between the plasma dynamics and the fields, these changes influence the macroscopic behavior of a magnetized plasma [2–5]. Of general interest are the cases characterized by low collisionality plasma regimes, in which reconnection is observed to occur over time scales much shorter than expected from resistive magneto-hydrodynamical (MHD) models [6].

A laboratory experiment, based on the Versatile Toroidal Facility (VTF) [7], was recently developed to address the question of which mechanisms can allow rapid changes of the magnetic field topology in collisionless plasmas. In this Letter we focus on mechanisms that are present at the level of single particle orbits, for relatively low values of the magnetic field perpendicular to the reconnection plane.

In general, the reconnection process leads to the formation of an X line, i.e., a line along which magnetic field lines crosslink. In our experiment, the magnetic X line is generated by external coils forming a toroidal magnetic cusp, a configuration that is relevant both to laboratory studies of driven magnetic reconnection [8–12] and to naturally occurring, self-consistent reconnection. The value of the electric field along the X line, which sustains the change of topology and, combined with the magnetic field, causes plasma drifts, corresponds to the reconnection rate. The electric field can be generated by an instability leading to a growing magnetic island, by an independent plasma flow, or can be externally driven, the case of the VTF experiment. In such a case the global, steady-state reconnection rate is imposed.

Particle orbits in Harris sheetlike magnetic field configurations [13], resembling the magnetic field in the earth's geomagnetic tail, have been studied intensively [14]. In contrast, despite its importance in the context of magnetic reconnection, only limited attention has been given to the particle orbits in a magnetic cusp.

The magnetic cusp configuration is produced on VTF by poloidal field coils installed outside the vacuum vessel, as shown in Fig. 1, which illustrates the experimental setup. Plasmas are produced via electron cyclotron resonance heating by applying up to 50 kW of rf power at a frequency of 2.45 GHz. For the maximal operational cusp field, the breakdown of the injected gas (normally Argon at 1×10^{-5} Torr) occurs on a ring centered on the X line and with a radius of 30 cm, where $B = 87.5$ mT. Highly reproducible target plasmas with density $n \simeq 1 \times 10^{17}$ m^{-3} and temperature $T_e \simeq 20$ eV are obtained. In addition to the cusp field, a guide field in the toroidal direction (0–200 mT) may be added. In the experiments reported herein, the magnitude of the guide field is kept between 20 and 80 mT. Reconnection is driven by inducing a toroidal electric field up to $E = 10$ V/m using an additional coil set, corresponding to loop voltages around the torus up to 65 V. Previous experiments have been performed on linear cusp configurations [15,16]. Three distinctive features characterize the VTF experiment: a

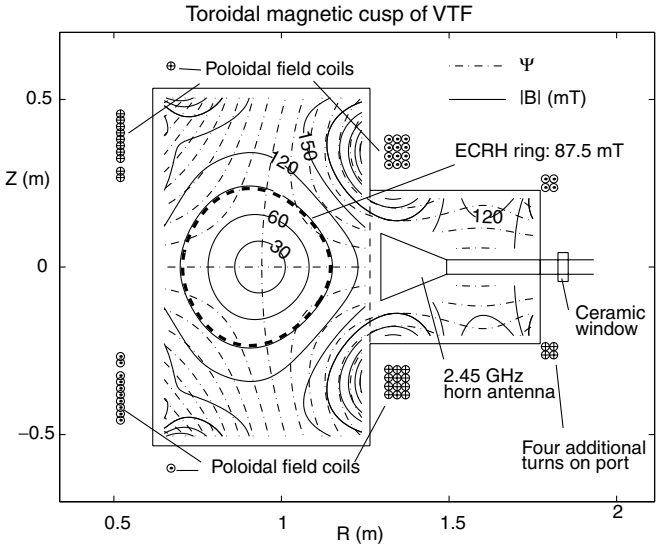

FIG. 1. Poloidal cross section of VTF. The solid contour lines represent the poloidal magnetic field strength. The dashed contour lines correspond to constant levels of the poloidal magnetic flux, Ψ, which coincide with magnetic field lines. Note that in the regimes described in this Letter the shape of the magnetic field lines is observed to remain unaltered during driven reconnection.

collisionless regime, with electron mean free paths much longer than the device size, a plasma production independent of the mechanism driving reconnection, and a guide field that can be varied over a wide range of values.

Despite the large loop voltage, for the regime considered in this Letter, $B_{\text{guide}}/\nabla B_{\text{cusp}} < 1$ m, no toroidal current channel is observed during the electric field pulses that drive reconnection. Both the macroscopic current measurements via a Rogovsky coil and the measurements of local magnetic flux via a multichannel magnetic probe covering the whole plasma cross section give upper limits for the current that are below 5 A. The experimentally reconstructed poloidal magnetic flux, operated with a spatial resolution of about 1 cm, does not differ from the vacuum flux shown in Fig. 1.

On the basis of this observation, the properties of particle orbits in the currentless cusp are investigated. Because of the relatively large aspect ratio of the VTF device, we consider for simplicity a linear cusp configuration, described by the magnetic vector potential

$$\mathbf{A} = \left(-\frac{1}{2}\, b_0 y l_0, \frac{1}{2}\, b_0 x l_0, b_0 xy \,-\, E_z t\right). \tag{1}$$

The coordinate system is selected such that the X line is in the z direction:

$$\mathbf{B} = \nabla \times \mathbf{A} = b_0(x\hat{\mathbf{x}} \,-\, y\hat{\mathbf{y}} \,+\, l_0\hat{\mathbf{z}}), \tag{2}$$

$$B = |\mathbf{B}| = b_0\sqrt{x^2 \,+\, y^2 \,+\, l_0^2}\,. \tag{3}$$

The magnetic flux in the xy plane reconnects at the rate corresponding to the homogeneous electric field in the z direction, $E_z = -\partial A_z/\partial t$. Note that $\nabla \times \nabla \times \mathbf{A} = 0$, consistently with the absence of macroscopic currents revealed by the experiment in this configuration.

The total energy is conserved for any particle in the magnetic cusp. For clarity, we consider separately the electrostatic potential self-generated on the plasma poloidal cross section, Φ, and the externally imposed electric field in the z direction,

$$\mathcal{E}_{\text{tot}} = \mathcal{E}_{\text{k}} \,-\, qE_z z \,+\, q\Phi\,. \tag{4}$$

Consistently with the toroidal symmetry of the experiment we assume that $\Phi = \Phi(x, y)$ is independent of z.

Following our experimental scenario, in this paper we consider only configurations for which the magnetic field in the z direction is strong enough that the magnetic moment, μ, is conserved at all locations [7] ($l_0 \gg \sqrt{mv/qb_0}$). Furthermore, we require that $E_z/B \ll v$, so that the particles are not demagnetized by the electric field.

From the conservation of μ and the requirement that the kinetic energy of a particle be greater than the energy associated with the motion perpendicular to B, we get the condition $\mathcal{E}_{\text{k}} \geq \mu B$. Since the magnetic field strength increases with the distance from the X line, the particles are "mirror" confined to the region

$$\sqrt{x^2 \,+\, y^2 \,+\, l_0^2} \leq \frac{\mathcal{E}_{\text{k}}}{\mu b_0}\,. \tag{5}$$

Although $\mathcal{E}_{\text{k}}$ is not conserved, in the case of finite electric field it is a bounded function of (x, y), and the mirror effect remains.

Figure 2(A) illustrates the particle motion derived for this configuration within the guiding center approximation [17,18], including the two leading orders in $\varepsilon = \rho_l/L$, where ρ_l is the Larmor radius and L is the length scale of variations in the magnetic field. The corresponding xz projection is shown in Fig. 2(B). The results obtained using the guiding center approximation, which will be used throughout the paper, have been validated by a comparison with particle orbits calculated from a full integration of the equation of motion for a linear cusp.

The main effect of the electric field is to cause the particle drift across the xy plane. The drift speed in the xy plane can be determined by considerations similar to those by Ware [19] regarding trapped particles in tokamaks. Let $\mathbf{r} = (x, y, z)$ and $\dot{\mathbf{r}} = (\dot{x}, \dot{y}, \dot{z})$ represent the guiding center location and velocity. Consistent with the guiding center equations [18], in the case considered here [$\mathbf{B} \cdot (\nabla \times \mathbf{B}) = 0$] the guiding center Lagrangian can be written as $L = (q\mathbf{A} + mv_{\parallel}\mathbf{B}/B) \cdot \dot{\mathbf{r}} - q\Phi(x, y)$ [20], where $v_{\parallel} = \pm\sqrt{2(\mathcal{E}_{\text{k}} - \mu B)/m}$ [$= \mathbf{v} \cdot \mathbf{B}/B + O(\varepsilon)$]. Since L is independent of z, the canonical momentum in the z direction,

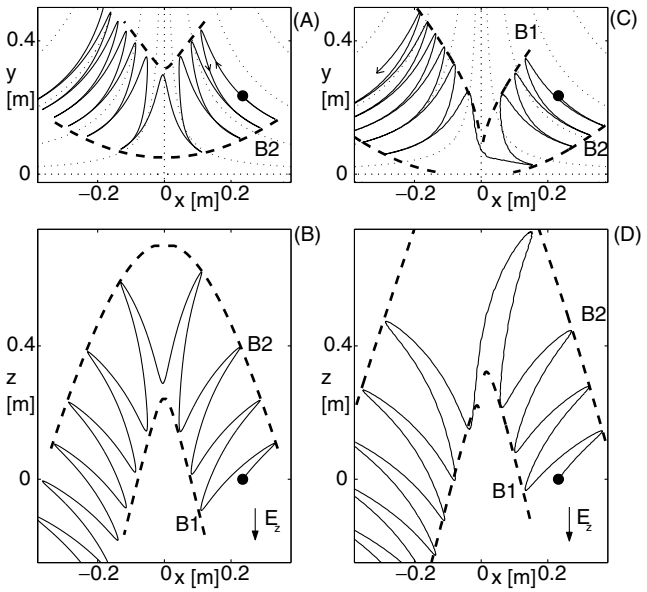

FIG. 2. Guiding center trajectory [in xy (A,C) and xz (B,D) projections] of a 15 eV ArII ion calculated for a linear cusp configuration, characterized by $b_0 = 0.3$ T/m, $l_0 = 0.3$ m, $E_z = -10$ V. The trajectory of (A,B) is calculated with $\Phi = 0$. The potential $\Phi = -E_z l_0 \log(x/y)/2$ is included for the trajectory of (C,D). The singularities in Φ were removed by smoothing Φ over 1 cm. The lines $B1$ and $B2$ represent the loci of the orbit bounce point as is obtained on the basis of the constants of motions $\mathcal{E}_{\text{tot}}$, μ, p_z, and J.

$$p_z = dL/d\dot{z} = qb_{0xy} - qE_z t + m v_\parallel \frac{B_z}{B} \tag{6}$$

is a constant of motion.

Because $v_\parallel = 0$ at the particle bounce points, we find that at these locations $p_z = qA_z$ and the particle bounce points are locked to the magnetic flux as the magnetic field lines sweep across the xy plane at the speed E_z/B_{xy}. Here $B_{xy} = b_0\sqrt{x^2 + y^2}$ is the field strength in the plane perpendicular to the X line. While in a tokamak only a fraction of the particles are subject to the Ware pinch, in the cusp plasma considered here all confined particles are trapped and hence subject to the velocity E_z/B_{xy}. This pinch drift velocity has been directly measured on the VTF plasmas [21].

This drift speed is independent of the potential Φ. In the case of Figs. 2(A) and 2(B) where $\Phi = 0$, the loci of the orbit bounce points are asymmetric around the line $x = y$. An analysis similar to that of [22] shows that in this case ∇B and curvature drifts are largely responsible for the drift across the xy plane.

In order to determine the loci of particle bounce points as a function of time, we consider the action integral $J = \oint v_\parallel \, dl$ over one particle bounce motion, where l represents the length measured along the field line. This is an adiabatic invariant and is conserved as the particle drifts with the field lines across the xy plane. Expanding in ε gives $J = J_0 + \varepsilon J_1 + \ldots$. In [18] it was shown that J_1 oscillates and vanishes at the orbit bounce points. Hence, the locations of the bounce points are fully determined by J_0 and the other constants of motions $\mathcal{E}_{\rm tot}$, μ, and p_z. Note that $J_0 = \oint \sqrt{2(\mathcal{E}_{\rm k} - \mu B)/m}\, dl$ is obtained by integration along field lines (not the guiding center orbit). For a particle following a magnetic field line passing though a point (x_0, y_0, z_0), we can express the z coordinate as a function of (x, y). Using Eq. (4), we obtain an expression for the kinetic energy as a function of (x, y):

$$\mathcal{E}_{\rm k}(x, y) = \mathcal{E}_{\rm tot} - q\Phi(x, y) + qE_{zz}(x, y), \tag{7}$$

$$z(x, y) = \frac{1}{2} l_0[\log(x/y) - \log(x_0/y_0)] + z_0. \tag{8}$$

Numerically the loci of the orbit bounce points are readily found as the lines where $\mathcal{E}_{\rm k} - B\mu$ vanishes for a given set of constants of motion p_z, $\mathcal{E}_{\rm tot}$, μ, and J.

The dashed curves $B1$ and $B2$ in Fig. 2 represent the loci of the orbit bounce points for the considered particle trajectory. Because of the positive work done by the electric field when the ion travels in the negative z direction [see Fig. 2(B)], the particle kinetic energy at the orbit bounce points along the loci $B1$ is larger than along $B2$. In the xy projection this is the cause of the asymmetry in the orbit around the line $x = y$, shifting the orbit towards higher value of y. In the case of electrons, the shift is towards higher values of x, so an electron injected in the same location as the ion considered above will cross the separatrix at a point along the line $y = 0$ and travel out though the quadrant $x > 0$ and $y < 0$. Therefore, in the absence of a finite electrostatic potential, the drift of the particles would cause macroscopic charge separation. Such unphysical macroscopic charge separation can be prevented by a finite electrostatic potential in the xy plane. The electrostatic potential prohibiting charge separation may be determined from Eq. (7).

We limit our analysis to electron and ion distribution functions that fulfill the condition $q_e \int f_e(\lambda, p_z, \mathcal{E}_{\rm k}, t)\, d\mathcal{E}_{\rm k} + q_i \int f_i(\lambda, p_z, \mathcal{E}_{\rm k}, t)\, d\mathcal{E}_{\rm k} = 0$. This implies quasineutrality for all values of the pitch angle $\lambda = \mu/\mathcal{E}_{\rm k}$. Hence, for any value of λ quasineutrality can be fulfilled only if the bounce points are symmetric around the lines $|x| = |y|$. This requires that the expression (7) be symmetric in $|x|$ and $|y|$.

The shape of the bounce point loci must be independent of q. The only electrostatic potential that guarantees these properties is that which exactly cancels the work of the electric field E_z for a particle following a magnetic field line:

$$\Phi(x, y) = \frac{E_z l_0 \log(x/y)}{2} + c_0(xy). \tag{9}$$

The electrostatic potential in the xy plane is hereby determined with the exception of $c_0(xy)$, which is a function of the magnetic flux, proportional to the product xy. With this potential, the kinetic energy of a particle is conserved at all points as the particle moves along the magnetic field line. The kinetic energy will change only on the time scale of the particle motion with the field lines across the xy plane. This drift speed, E_z/B_{xy}, is independent of Φ.

The electrostatic potential given by Eq. (9) (with $c_0 = 0$) was included in the calculation of the guiding center trajectory and the loci of the orbit bounce points shown in Figs. 2(C) and 2(D). In the xy projection [Fig. 2(C)] we note how the loci $B1$ and $B2$ are symmetrically located around the line $x = y$. As the particle crosses the separatrix, the value of J is increased. This causes the change in the distance between the loci of the bounce points for $x < 0$. Ions may now cross the separatrix for $y = 0$ and drift out through the quadrant $x > 0, y < 0$. Which of the two quadrants the ion drifts into depends on the phase in the bounce motion between $B1$ and $B2$, in turn determined by initial conditions. In Fig. 2(D) it is seen that the particle experiences an overall drift in the positive z direction as it approaches the X line, against the force of the electric field E_z.

In order to prove the validity of these arguments experimentally, the plasma potential profile of the VTF plasma was measured in a number of discharges during driven reconnection using a set of radially moving electrostatic probes. For each point, two configurations with identical target plasmas but with the induced electric field in opposite directions were considered. The modification on the electrostatic potential ΔV_p due to the reconnection process was determined by subtracting the two profiles. Figure 3(top) shows the measured and theoretical values of ΔV_p for a part of the plasma cross section. The dashed

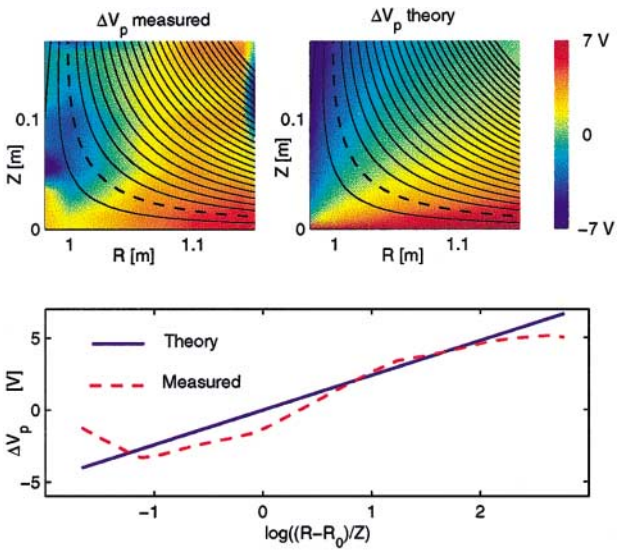

FIG. 3 (color). Measured and theoretical change in plasma potential during reconnection in a VTF plasma.

line in Fig. 3(bottom) shows the potential ΔV_p measured along the field line $xy = 0.02$ m^2 [this is the dashed field line in Fig. 3(top)] as a function of $\log(x/y)$. The full line shows the potential calculated from Eq. (9). At all locations (away from the separatrix) where the temperature and density profiles are observed to be unperturbed by the reversion of the reconnection drive, the measured change in plasma potential is consistent with the result obtained on the basis of single particle motion, expressed in (9).

In summary, we have found analytically and demonstrated experimentally that reconnection driven by an electric field along the X line can take place in a collisionless plasma, in a magnetic cusp with a relatively weak guide field, without a macroscopic current layer, consistently with the effect of particle orbits. Three main conclusions can be highlighted.

First, because particles are mirror trapped, the reconnection electric field, E_z, does not accelerate the particles along the X line. This allows the reconnection to proceed at the externally imposed rate, the same as in vacuum. Note that this neoclassical effect becomes important in the collisionless regime, and is not inconsistent with the departures from rates predicted by Sweet-Parker models that include classical resistivity, observed when the collisionless regime is approached in other laboratory experiments [8,9].

Second, particles drift across the plane perpendicular to the X line at the Ware-pinch velocity (E_z/B_{xy}). In the case where $\Phi(x, y)$ is given by Eq. (9), the loci of the bounce points are symmetric, and averaged over an orbit bounce motion the effects of ∇B and curvature drifts vanish. For this case the drift across the xy plane is accounted for by the drift $\mathbf{v}_{E\times B} = \mathbf{E} \times \mathbf{B}/B^2$, and it follows that $\mathbf{E} + \mathbf{v}_{E\times B} \times \mathbf{B} = 0$. This "frozen in law" at the single particle level is expected to break along the separatrix where different mechanisms can remove the steep gradients in Φ. Higher resolution measurements of the structure of the electrostatic potential will be necessary to identify such mechanisms.

Third, an electrostatic potential given by Eq. (9) is necessary to avoid charge separation. This potential was calculated analytically and has been measured experimentally for the first time. The nature of particle orbits does not allow a net plasma energization for the scenario considered here. However, the potential that develops in the reconnection plane could act as a plasma energization process in the case of a very strong guide field, as suggested by particle simulations [23,24]. Further investigations are planned to explore this heating mechanism, along with the formation of a macroscopic current layer in the case of a strong guide field, suggested by preliminary experiments on VTF [21].

The authors would like to thank A. Scarabosio, C. Lemmerz, E. Fitzgerald, D. Gwinn, and W. Parkin for technical help, and M. Porkolab for support with the experiments. This work is partly funded by DoE Junior Faculty Development Award No. DE-FG02-00ER54601.

[1] J. W. Dungey, Philos. Mag. **44**, 725 (1953).
[2] J. B. Taylor, Rev. Mod. Phys. **28**, 243 (1986).
[3] V. M. Vasyliunas, Rev. Geophys. Space Phys. **13**, 303 (1975).
[4] T. D. Phan *et al.,* Nature (London) **404**, 848–850 (2000).
[5] S. Masuda, T. Kosugi, H. Hara, and Y. Ogawara, Nature (London) **371**, 495 (1994).
[6] R. M. Kulsrud, Phys. Plasmas **2**, 1735 (1995).
[7] J. Egedal, A. Fasoli, M. Porkolab, and D. Tarkowski, Rev. Sci. Instrum. **71**, 3351 (2000).
[8] Y. Ono, M. Inomoto, T. Okazaki, and T. Ueda, Phys. Plasmas **4**, 1953 (1997).
[9] M. Yamada, H. T. Ji, S. Hsu, T. Carter, R. Kulsrud, N. Bretz, F. Jobes, Y. Ono, and F. Perkins, Phys. Plasmas **4**, 1936 (1997).
[10] C. G. R. Geddes, T. W. Kornack, and M. R. Brown, Phys. Plasmas **5**, 1027 (1998).
[11] M. Yamada, H. T. Ji, S. Hsu, T. Carter, R. Kulsrud, Y. Ono, and F. Perkins, Phys. Rev. Lett. **78**, 3117 (1997).
[12] Y. Ono, M. Yamada, T. Akao, T. Tajima, and R. Matsumoto, Phys. Rev. Lett. **76**, 3328 (1996).
[13] E. G. Harris, Nuovo Cimento **23**, 1167 (1962).
[14] J. Chen, J. Geophys. Res. **97**, 15 011 (1992).
[15] R. L. Stenzel and W. Gekelmann, J. Geophys. Res. **87**, 101 (1982).
[16] A. G. Frank, Plasma Phys. Controlled Fusion **41**, A687 (1999).
[17] R. G. Littlejohn, J. Plasma Phys. **29**, 111(1983).
[18] T. G. Northrop, C. S. Liu, and M. D. Kruskal, Phys. Fluids **9**, 1503 (1966).
[19] A. A. Wate, Phys. Rev. Lett. **25**, 15 1970).
[20] A. I. Morozov and L. S. Solev'ev, Rev. Plasma Physics (Plenum, New York, 1966), Vol. 2, pp. 226–230.
[21] J. Egedal, A. Fasoli, D. Tarkowski, and A. Scarabosio, Phys. Plasmas **8**, 1935 (2001).
[22] M. G. Haines and P. Martin, Phys. Plasmas **3**, 4536 (1996).
[23] R. Horiuchi and T. Sato, Phys. Plasmas **4**, 277 (1997).
[24] Y. E. Litvinenko, Phys. Plasmas **4**, 3439 (1997).